
Cluster approximations for the TASEP: stationary state and dynamical transition

A. PELIZZOLA^{1,2} AND M. PRETTI^{1,3}

¹ *Dipartimento di Scienza Applicata e Tecnologia and CNISM, Politecnico di Torino, Corso Duca degli Abruzzi 24, I-10129 Torino, Italy*

² *INFN, Sezione di Torino, via Pietro Giuria 1, I-10125 Torino, Italy*

³ *Consiglio Nazionale delle Ricerche-Istituto dei Sistemi Complessi (CNR-ISC)*

PACS 02.50.Ga – Markov processes
PACS 05.50.+q – Lattice theory and statistics (Ising, Potts, etc.)
PACS 89.75.-k – Complex systems

Abstract – We develop and test cluster approximations, which generalize simple mean-field by taking into account more and more local correlations, for the Totally Asymmetric Simple Exclusion Process with open boundaries. We consider in detail the pair and triplet approximations, discussing the improvements with respect to mean field in various steady state properties. Moreover, we analyze the recently discovered dynamical transition, describing how the spectrum of the relaxation matrix changes at the transition.

Introduction. – In equilibrium statistical physics a huge research effort has been devoted to develop approximations for models with a large number of interacting variables, whose exact solution is typically out of reach for both analytical and computational approaches. A large fraction of this effort has been focused on mean field techniques and their generalizations, yielding simple and efficient approaches, which can turn out to be exact in certain limiting cases.

In the last decades such an effort has been extended to nonequilibrium statistical physics, in particular to the well defined and interdisciplinarily relevant problem of models defined on graphs, whose dynamics can be described in terms of a Markov process [1], paradigmatic examples being the kinetic Ising model and epidemic processes.

A lot of techniques exist, which go beyond the simple mean-field approach [2]. Here we briefly mention those which are most relevant for the present work, for a more detailed review see [3]. In many such approaches one assumes that the probability distribution of a model with many variables factors into a suitable product of local marginals, including of course mean-field as its simplest version. This idea has led to the so-called cluster approximations [4,5], local structure theories [6,7], n -step Markovian approximations [8], and local equilibrium approximations [2,9–12]. The Path Probability Method (PPM) [13–17] is the dynamical version of the well-known Cluster

Variational Method [18–20] and, like the latter, is based on the minimization of a suitable free-energy-like functional obtained by a cluster expansion. It has been shown to be related, in certain instances, to local equilibrium approximations [21]. The well-known cavity method [22] has been recently extended to kinetic problems [23–29] yielding approaches known as dynamic cavity and dynamic message passing [30], which have been shown to be efficient and accurate on large systems. In the last few years, suitable generalizations of the PPM idea have been shown [31–33] to be often more efficient and accurate than dynamic cavity and dynamic message passing. Although based on a cluster expansion of a free-energy-like functional, these approaches can in some instances be interpreted in terms of an assumption of a suitable factorization of the model probability distribution, as in local equilibrium approximations.

Some of the aforementioned approaches are not directly applicable to another class of paradigmatic models in nonequilibrium statistical physics, namely the Totally Asymmetric Simple Exclusion Process (TASEP) and its extensions (see [34] for a recent review of these models and their applications). This can be understood by considering the formulation of the dynamics. In both kinetic Ising-like models and epidemic processes, a transition at a given node (e.g. from susceptible to infected) can occur without implying a transition on an adjacent node. In the

TASEP we have particles moving on a one-dimensional lattice, and a particle can hop to the adjacent node provided it is empty, so the transition from occupied to empty at node i implies the transition from empty to occupied at node $i + 1$.

In the present work we shall apply cluster approximations of the local equilibrium type to the TASEP model. We shall explicitly consider the pair and triplet approximations, corresponding to the (2, 1) and (3, 2) approximations in [4], or the “triplet” and “quintuplet” approximations in [12], which take into account correlations between 2 and 3 adjacent nodes respectively. In addition to discussing how these approximations can improve the description of steady-state properties, we shall focus on a recently discovered dynamical transition. In this case, before applying the pair and triplet approximations, we shall investigate in detail the mean field approximation, discussing in particular the qualitative changes occurring at the transition in the spectrum of the relaxation matrix.

Model. – The TASEP is a paradigmatic model in nonequilibrium statistical physics. It was originally introduced, in a more general form, in [35] as a model of mRNA translation. The steady state of the TASEP with open boundaries [36] has been exactly worked out in the 1990s [37–40], showing a rich phase diagram, features which make it a suitable candidate for testing approximate methods. The mean-field approximation for the steady state was discussed in [37]. As previously mentioned, the model is defined on a one-dimensional lattice, where particles can hop only rightward, from each node to the adjacent one, provided the latter is empty, at unit rate. Considering a lattice of length N , we label lattice nodes from left to right by $i = 1, \dots, N$ and introduce random variables of the occupation number type $n_i^t = 0, 1$, where as customary $n_i^t = 1$ if node i is occupied by a particle at time t and $n_i^t = 0$ otherwise. Expectation values will be denoted by $\langle \rangle$, e.g. we will use the local densities $\rho_i^t = \langle n_i^t \rangle$. Local densities in the stationary state do not depend on time and will be denoted by ρ_i . Whenever the stationary density profile exhibits a bulk region, we will denote the corresponding density by ρ .

Various types of boundary conditions have been considered in the literature. Here we will focus on the particularly interesting case of open boundary conditions, with particles injected at the leftmost node (provided it is empty) with rate α , and extracted from the rightmost node (provided it is occupied) with rate β . Notice that a fully equivalent description may be obtained assuming that the system is in contact with two reservoirs of fixed densities α and $1 - \beta$, which respectively inject and extract particles at unit rate.

Upon varying α and β a rich, exactly known [37–42] phase diagram, illustrated in Fig. 1, is obtained.

If $\beta < 1/2$, $\alpha > \beta$, the steady state is in a *high density phase*, with a current $J = \beta(1 - \beta)$ and a bulk density $\rho = 1 - \beta > 1/2$, which extends up to the right boundary.

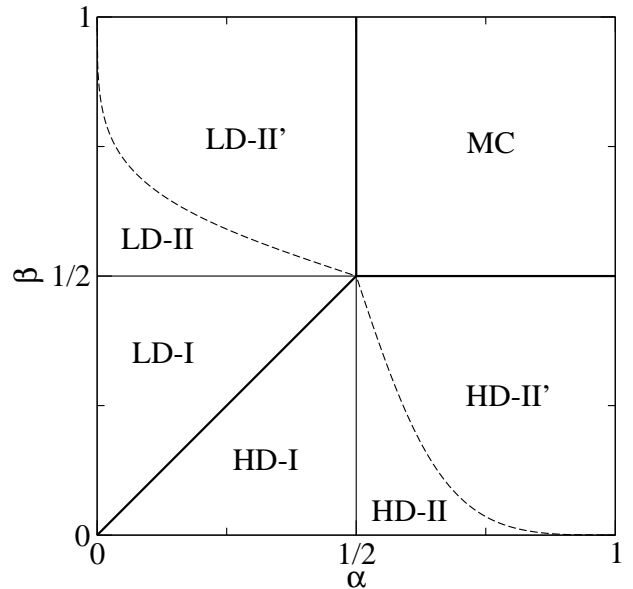


Fig. 1: Phase diagram of the TASEP model with open boundary conditions. See main text for a description of the various phases and transitions between them.

At the left boundary the density takes the value $1 - J/\alpha$ and approaches the bulk with an exponential decay (in the region denoted by HD-I in Fig. 1), with power-law corrections for $\alpha \geq 1/2$ (regions denoted by HD-II and HD-II' in Fig. 1).

Exploiting a particle-hole symmetry of the model, it can be understood that for $\alpha < 1/2$, $\beta > \alpha$, the situation is reversed: the steady state is in a *low density phase*, with $J = \alpha(1 - \alpha)$ and $\rho = \alpha < 1/2$, which extends up to the left boundary, while at the right boundary the density takes the value J/β and approaches the bulk with an exponential decay (in the region denoted by LD-I in Fig. 1), with power-law corrections for $\beta \geq 1/2$ (regions denoted by LD-II and LD-II' in Fig. 1).

The above 2 phases are separated by the coexistence line $0 < \alpha = \beta < 1/2$ (the thick line separating LD-I and HD-I regions in Fig. 1), where the current is $J = \alpha(1 - \alpha)$ and the densities at the left and right boundaries are α and $1 - \alpha$ respectively, and are connected by a linear density profile.

Finally, for $\alpha > 1/2$ and $\beta > 1/2$ the steady state is in a *maximal current phase* (denoted by MC in Fig. 1), with $J = 1/4$ and $\rho = 1/2$. The densities at the left and right boundaries are $1 - J/\alpha > 1/2$ and $J/\beta < 1/2$ respectively, and the approach to the (central) bulk value is power-law on both sides.

In addition to the above phases and transitions, a *dynamical phase transition* (denoted by dashed lines in Fig. 1), not corresponding to any steady-state transition, has recently been discovered theoretically [41, 42] (and numerically confirmed [43]) in the low and high density phases. Considering the high density phase to fix ideas, the transition can be characterized as follows: for any $\beta < 1/2$,

the (longest) relaxation time of the system is independent of α for $\alpha > \alpha_c(\beta)$ (the region denoted by HD-II' in Fig. 1), where

$$\alpha_c(\beta) = \left[1 + \left(\frac{\beta}{1-\beta} \right)^{1/3} \right]^{-1}, \quad (1)$$

while for $\alpha < \alpha_c(\beta)$ the relaxation time depends on both α and β .

Cluster approximations. – Simple mean-field-like, cluster-based approximations can be obtained by assuming that, at a given time t , the model probability distribution factors as a suitable product of local marginals.

To be more quantitative, it is useful to define a class of marginals, involving a string of $k+1$ (with $k \geq 0$) adjacent nodes: $P_i^t[n_i n_{i+1} \cdots n_{i+k}]$ will denote the probability that, at time t , the occupation numbers of nodes from i to $i+k$ take values $n_i, n_{i+1}, \dots, n_{i+k}$ respectively. In order to model boundary conditions we will introduce two auxiliary nodes $i=0$ and $i=N+1$ of fixed densities $\rho_0 = \alpha$ and $\rho_{N+1} = 1 - \beta$ respectively, and we will assume

$$P_0^t[1n_1 \dots n_i] \equiv \alpha P_1^t[n_1 \dots n_i], \quad i = 1, \dots, N \quad (2)$$

and

$$P_i^t[n_i \dots n_N 0] \equiv \beta P_i^t[n_i \dots n_N], \quad i = 1, \dots, N. \quad (3)$$

It is immediate to write exact dynamical evolution equations for a few of the above marginals. The time evolution of the local densities $\rho_i^t = P_i^t[1]$ is given by

$$\dot{P}_i^t[1] = P_{i-1}^t[10] - P_i^t[10], \quad i = 1, \dots, N, \quad (4)$$

where the local currents $J_i^t = P_i^t[10]$ appear. The time evolution of the local currents is in turn given by

$$\dot{P}_i^t[10] = P_{i-1}^t[100] - P_i^t[10] + P_i^t[110], \quad i = 1, \dots, N-1, \quad (5)$$

where certain 3-node marginals appear. The time evolution of these 3-node marginals is then given by

$$\begin{aligned} \dot{P}_i^t[100] &= P_{i-1}^t[1000] - P_i^t[100] + P_i^t[1010], \\ \dot{P}_i^t[110] &= P_{i-1}^t[1010] - P_i^t[110] + P_i^t[1110] \end{aligned} \quad (6)$$

($i = 1, \dots, N-2$) and involves 4-node marginals, and so on. Clearly, in order to close our set of equations, we need to introduce approximations.

The simplest possible choice is the ordinary mean-field approximation [37], where one assumes that

$$P_i^t[n_i n_{i+1}] = P_i^t[n_i] P_{i+1}^t[n_{i+1}]. \quad (7)$$

Using this assumption in Eq. 4 we obtain a set of closed equations for the local densities:

$$\dot{\rho}_i^t = \begin{cases} \rho_{i-1}^t(1 - \rho_i^t) - \rho_i^t(1 - \rho_{i+1}^t), & i = 2, \dots, N-1 \\ \alpha(1 - \rho_1^t) - \rho_1^t(1 - \rho_2^t), & i = 1 \\ \rho_{N-1}^t(1 - \rho_N^t) - \beta\rho_N^t, & i = N. \end{cases} \quad (8)$$

Pair approximation. A second, more accurate, level of approximation is obtained by retaining correlations between adjacent nodes, that is by assuming

$$P_i^t[n_i n_{i+1} n_{i+2}] = \frac{P_i^t[n_i n_{i+1}] P_{i+1}^t[n_{i+1} n_{i+2}]}{P_{i+1}^t[n_{i+1}]} \quad (9)$$

as in the (2, 1) approximation in [4] or in the ‘‘triplet’’ approximation in [12]. In order to obtain a set of dynamical evolution equations for the $2N-1$ variables $\{\rho_i^t, J_i^t\}$, we first observe that Eq. 4 can be rewritten, with no need of approximations, as

$$\dot{\rho}_i^t = \begin{cases} J_{i-1}^t - J_i^t, & i = 2, \dots, N-1 \\ \alpha(1 - \rho_1^t) - J_1^t, & i = 1 \\ J_{N-1}^t - \beta\rho_N^t, & i = N. \end{cases} \quad (10)$$

In addition, we close Eq. 5 using the approximation Eq. 9, obtaining

$$j_i^t = \frac{J_{i-1}^t(1 - \rho_{i+1}^t - J_i^t)}{1 - \rho_i^t} - J_i^t + \frac{(\rho_i^t - J_i^t)J_{i+1}^t}{\rho_{i+1}^t} \quad (11)$$

for $i = 2, \dots, N-1$,

$$j_1^t = \alpha(1 - \rho_2^t - J_1^t) - J_1^t + \frac{(\rho_1^t - J_1^t)J_2^t}{\rho_2^t}, \quad (12)$$

and

$$j_{N-1}^t = \frac{J_{N-2}^t(1 - \rho_N^t - J_{N-1}^t)}{1 - \rho_{N-1}^t} - J_{N-1}^t + \beta(\rho_{N-1}^t - J_{N-1}^t). \quad (13)$$

Triplet approximation. A third level of approximation is obtained by retaining correlations between 3 adjacent nodes, that is by assuming

$$P_i^t[n_i n_{i+1} n_{i+2} n_{i+3}] = \frac{P_i^t[n_i n_{i+1} n_{i+2}] P_{i+1}^t[n_{i+1} n_{i+2} n_{i+3}]}{P_{i+1}^t[n_{i+1} n_{i+2}]} \quad (14)$$

as in the (3, 2) approximation in [4] or in the ‘‘quintuplet’’ approximation in [12]. Using the above assumption in Eqs. 6 we obtain equations which, together with Eqs. 4 and 5, form a closed set, involving $4N-5$ variables. Calculations at the triplet level are straightforward, though cumbersome, extensions of the pair approximation ones. In the following, in order to keep our presentation contained, we will mainly focus on the pair approximation, but we will comment on the main changes at the triplet level and of course present the corresponding results.

Steady state in the pair and triplet approximations. The equations derived above for the pair approximation, in particular Eqs. 10 and 11–13, can be directly used to describe the steady state of the model. In the steady state, the variables $\{\rho_i^t, J_i^t\}$ become time-independent. From the continuity equation Eq. 10 we obtain

$$J_i = J_{i-1}, \quad i = 2, \dots, N-1, \quad (15)$$

meaning that the stationary current is site-independent (so that we shall denote it by $J = J_i$, $i = 1, \dots, N-1$), together with the boundary conditions

$$\rho_1 = 1 - \frac{J}{\alpha}, \quad \rho_N = \frac{J}{\beta}. \quad (16)$$

In addition, from Eqs. 11–13 and using the above boundary conditions (which happen to be exact), we obtain the (approximate) recursive equation

$$\rho_{i+1}(\rho_{i+1} - \rho_i + J) = (1 - \rho_i)(\rho_i - J), \quad (17)$$

which holds for $i = 1, \dots, N-1$ and can be solved w.r.t. ρ_{i+1} , obtaining

$$\rho_{i+1} = \frac{\rho_i - J}{2} \left(1 + \sqrt{1 + 4 \frac{1 - \rho_i}{\rho_i - J}} \right). \quad (18)$$

Of course, one could also solve w.r.t. ρ_i and obtain the inverse of the above recursion. These recursions have the same fixed points

$$\rho_{\pm} = \frac{1 \pm \sqrt{1 - 4J}}{2} \quad (19)$$

as in mean-field, and hence the bulk density ρ and the current J satisfy the exact relation $J = \rho(1 - \rho)$.

A numerical solution of Eq. 18 with the boundary conditions Eq. 16 yields the density profiles in the various phases of the model. The phase diagram turns out to coincide with the mean-field one (which is known to be exact), but of course one can obtain better approximations for the density profiles. In particular, in the low-density phase ($\alpha < 1/2$, $\beta > \alpha$, bulk density $\rho = \alpha < 1/2$, boundary densities $\rho_1 = \alpha$ and $\rho_N = \alpha(1 - \alpha)/\beta$, and current $J = \alpha(1 - \alpha) < 1/4$), the approach to the bulk density (from the right) is exponential, as in mean-field, but with a better approximation for the characteristic length. Setting $x_i = \rho_i - \rho$ we find $x_{i+1} = \gamma x_i$, where

$$\gamma \equiv \gamma(\rho) = \frac{1 - \rho^2}{\rho(2 - \rho)}, \quad (20)$$

corresponding to a characteristic length ξ given by

$$\xi^{-1} = \ln \gamma(\alpha). \quad (21)$$

In the triplet approximation the approach to the bulk is described in terms of x_i and the 2 additional quantities

$$\begin{aligned} y_i &= P_i[100] - \rho(1 - \rho)^2, \\ z_i &= P_i[110] - \rho^2(1 - \rho), \end{aligned}$$

where the superscript denoting time has been dropped in the stationary state marginals. Linearizing close to the bulk we obtain

$$\begin{pmatrix} x_{i+1} \\ y_i \\ z_i \end{pmatrix} = \Gamma \begin{pmatrix} x_i \\ y_{i-1} \\ z_{i-1} \end{pmatrix}, \quad (22)$$

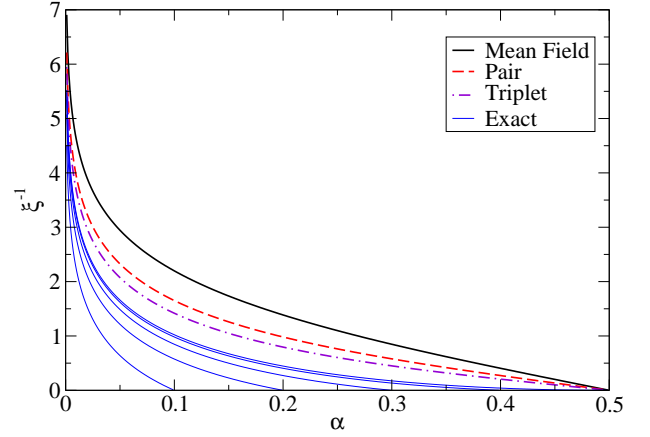


Fig. 2: Inverse characteristic length vs. α in the low-density phase. From top to bottom: mean-field approximation (full line), pair approximation (dashed), triplet (dot-dashed), exact results (thin full lines) for $\beta > 1/2$, $\beta = 0.4, 0.3, 0.2, 0.1$.

where

$$\Gamma(\rho) = \frac{1}{\rho(2-\rho)} \begin{pmatrix} 2\rho(1-\rho) & -(2-\rho) & -(1-\rho) \\ 2-\rho[5-3\rho(2-\rho)] & (2-\rho)(3-\rho) & 2(1-\rho)^2 \\ 0 & -\rho(2-\rho) & 0 \end{pmatrix}, \quad (23)$$

from which the inverse characteristic length ξ^{-1} can be obtained as the logarithm of the second smallest eigenvalue of Γ . The smallest eigenvalue turns out to be less than 1, which corresponds to an attractive direction of the low-density fixed point, but one can verify that any non-zero contribution along this direction is forbidden by the boundary conditions on the right side. This implies that some care is needed when solving numerically the equations for the density profile.

The (inverse) characteristic lengths estimated by the pair and triplet approximations are plotted in Fig. 2 and compared with the mean-field result $\xi^{-1} = \ln \frac{1-\alpha}{\alpha}$ and with the exact result $\xi^{-1} = \xi_{\alpha}^{-1} - \xi_{\beta}^{-1}$ (for $\beta < 1/2$) or $\xi^{-1} = \xi_{\alpha}^{-1}$ (for $\beta > 1/2$), where $\xi_{\sigma}^{-1} = -\ln[4\sigma(1-\sigma)]$ for $\sigma = \alpha, \beta$. Notice that the pair and triplet approximations, as well as mean field, are not able to reproduce the β dependence of the characteristic length for $\beta < 1/2$.

In Fig. 3 we report the density profiles, and compare them to the mean field and exact ones, for $N = 50$, $\alpha = 0.2$ and $\beta = 0.3$.

We do not show the equivalent of Figs. 2–3 in the high-density phase since they would be simply qualitatively symmetrical, due to the aforementioned particle-hole symmetry of the model, which is preserved by the approximate theory. We just mention that the characteristic length is given by

$$\xi^{-1} = -\ln \gamma(1 - \beta) = \ln \gamma(\beta), \quad (24)$$

where the latter equality easily follows from Eq. 20.

The two low- and high-density phases are separated by the coexistence line $\alpha = \beta < 1/2$. The density profile is symmetric and in the large N limit it exhibits

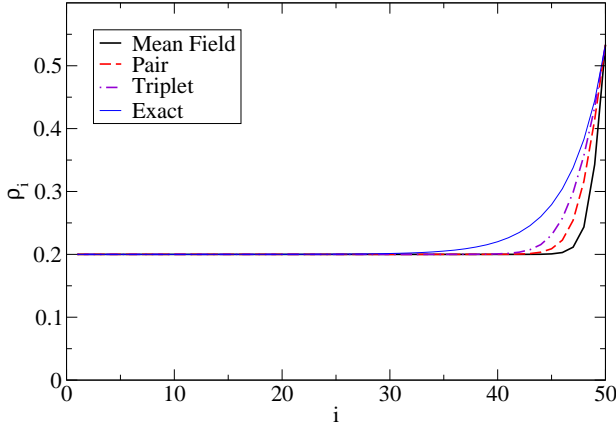


Fig. 3: Density profiles for $N = 50$, $\alpha = 0.2$, $\beta = 0.3$, (low-density phase). From bottom to top: mean field (full line), pair approximation (dashed), triplet (dot-dashed), exact result (thin full line).

2 macroscopic (“bulk”) regions, separated by a domain wall: a low-density one, with density $\rho_- = \alpha$, extending to the left boundary, and a high-density one, with density $\rho_+ = 1 - \beta$, extending to the right. The current is $J = \alpha(1 - \alpha) = \beta(1 - \beta)$ and the approach to both macroscopic regions is exponential, with a unique characteristic length which can be obtained by Eq. 21 or, equivalently, Eq. 24. In the limit $N \rightarrow \infty$ the domain wall can be anywhere and an infinite number of solutions appear. This result is the same as in the mean field approximation, while the exact solution averages over all the positions of the domain wall, yielding a linear density profile.

Finally, for $\alpha > 1/2$ and $\beta > 1/2$ we recover the **maximal current** phase, with bulk density $\rho = 1/2$, current $J = 1/4$ and boundary densities $\rho_1 = 1 - 1/(4\alpha) > 1/2$ and $\rho_N = 1/(4\beta) < 1/2$. In order to understand how the bulk density is approached from both sides, we need to expand Eq. 17 to 2nd order in x_i, x_{i+1} , obtaining

$$x_{i+1} - x_i \simeq -\frac{4}{3}x_i^2, \quad (25)$$

which is solved by $x_i \sim i^{-1}$ (or, from the right, $x_i \sim (N - i)^{-1}$). This i^{-1} behaviour, also given by the triplet approximation, is qualitatively the same as in the mean field approximation, while the exact solution gives also a power law, but with an exponent $1/2$ instead of 1. In Fig. 4 we report the density profiles in the pair and triplet approximations, and compare them to the mean field and exact ones, for $N = 499$ (using odd N is technically convenient because it allows to start the recursions from $\rho_{(N+1)/2} = 1/2$) and $\alpha = \beta = 1$. Due to the finite size, the current is slightly larger than $1/4$, in particular $J \simeq 0.2500218$ in the pair approximation and $J \simeq 0.2500380$ in the triplet approximation, to be compared with the exact result 0.2507508 and the mean field one 0.2500097 .

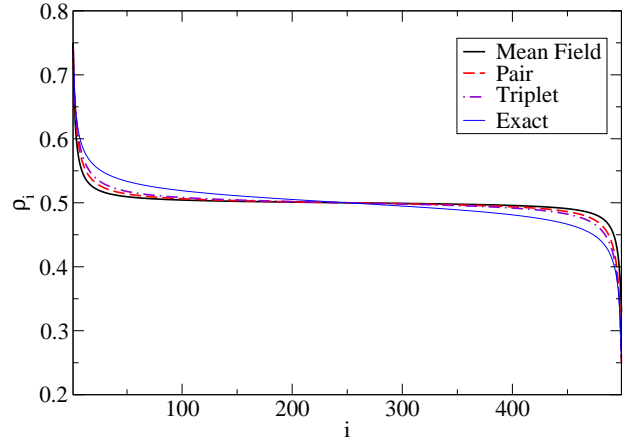


Fig. 4: Density profiles for $N = 499$, $\alpha = \beta = 1$, corresponding to the maximal current phase. Mean field (full line), pair approximation (dashed), triplet (dot-dashed), exact result (thin full line).

Dynamical transition in the mean field approximation.

The approach to the steady state can be quantitatively studied by linearizing the mean field dynamical equations, Eq. 8, close to their steady state fixed point. Denoting by ρ_i the steady state value of ρ_i^t and linearizing we have

$$\dot{\rho}_i^t = - \sum_{j=1}^N M_{ij}(\rho_j^t - \rho_j), \quad i = 1, \dots, N. \quad (26)$$

The matrix M characterizes relaxation. In particular, its smallest eigenvalue is the slowest relaxation rate, that is the inverse of the longest relaxation time. The numerical computation of its spectrum is particularly easy, since M is tridiagonal with elements

$$\begin{aligned} M_{i,i} &= \frac{J}{\rho_i(1 - \rho_i)}, & i = 1, \dots, N, \\ M_{i,i+1} &= -\frac{J}{1 - \rho_{i+1}}, & i = 1, \dots, N - 1, \\ M_{i,i-1} &= -\frac{J}{\rho_{i-1}}, & i = 2, \dots, N. \end{aligned} \quad (27)$$

Considering the high-density phase to fix ideas, we observe that in the large N limit, except for its small i (i.e. top-left) portion, M takes the Toeplitz form

$$M = \begin{pmatrix} \ddots & \ddots & & & \\ \ddots & \ddots & & & \\ \ddots & \ddots & & -(1 - \beta) & \\ & & -\beta & 1 & \end{pmatrix}. \quad (28)$$

The eigenvalues and eigenvectors of a tridiagonal Toeplitz matrix are well-known (see e.g. [44]). With the elements in Eq. 28 the eigenvalues are given by

$$\lambda_k = 1 - 2\sqrt{\beta(1 - \beta)} \cos \frac{k\pi}{N+1} = 1 - 2\sqrt{J} \cos \frac{k\pi}{N+1}, \quad (29)$$

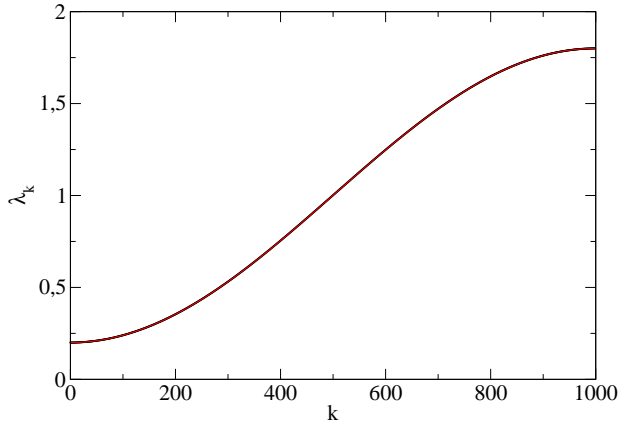


Fig. 5: Eigenvalues of the mean-field relaxation matrix (circles), compared with the eigenvalues of the corresponding Toeplitz matrix (line), for $\alpha = 1$, $\beta = 0.2$ and $N = 1000$.

for $k = 1, \dots, N$, and the smallest one tends to

$$\lambda_1 = 1 - 2\sqrt{\beta(1-\beta)} = 1 - 2\sqrt{J}. \quad (30)$$

This spectrum is functionally similar (though with different coefficients) to that given by the Domain Wall Theory (DWT) [45, 46].

One could wonder whether, at least in some cases, the spectrum of M is dominated by its Toeplitz-like macroscopic portion. Indeed, this is what we find for α larger than a certain threshold $\alpha_c(\beta)$ (to be determined later), which defines a region in the mean-field phase diagram corresponding to HD-II' in Fig. 1. In Fig. 5 we report the (numerically evaluated) eigenvalues of the mean field relaxation matrix Eq. 27 (black circles), together with the eigenvalues (Eq. 29) of the corresponding Toeplitz matrix (red line), for $\alpha = 1$, $\beta = 0.2$ and $N = 1000$. No differences are seen on the scale of the figure, the largest (absolute) difference is slightly less than $4 \cdot 10^{-4}$. Moreover, in Fig. 6 we report the (numerically evaluated) smallest eigenvalue λ_1 of the mean field relaxation matrix (black circles), together with the analytical estimate Eq. 30 (red line) for $\alpha = 1$ and $N = 200$, as a function of β . Again, we see perfect agreement. Notice that the analytical estimate Eq. 30 tends to the result given by the Burgers equation [43] approximation as β approaches $1/2$, but in general is different from this result.

The above situation changes qualitatively for $\alpha \in (\beta, \alpha_c(\beta))$, that is in a region of the mean-field phase diagram corresponding to HD-I and HD-II in Fig. 1. In addition to a “band” of $N - 1$ Toeplitz-like eigenvalues $\lambda_k \in (1 - 2\sqrt{J}, 1 + 2\sqrt{J})$, $k = 2, \dots, N$, distributed with the same density as for $\alpha > \alpha_c(\beta)$, we have that the smallest eigenvalue $\lambda_1 < 1 - 2\sqrt{J}$, which gives the slowest relaxation rate, detaches from the others. See Fig. 8 for the behaviour of the smallest eigenvalue in the case $\beta = 0.2$, compared to the pair and triplet approximations (see below) and the exact and DWT results.

In Fig. 7 we plot the components v_i of the eigenvector

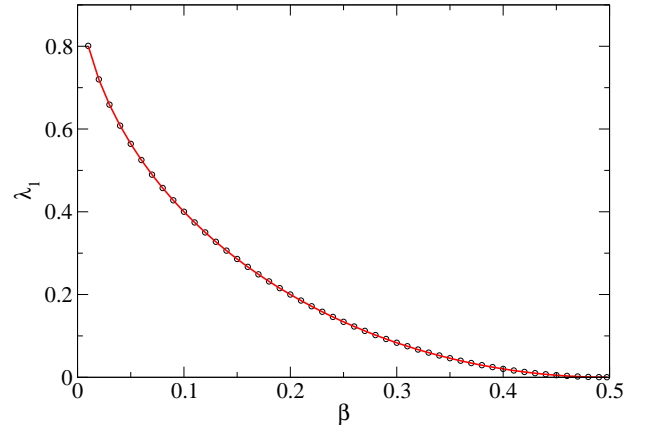


Fig. 6: Smallest eigenvalue of the mean-field relaxation matrix (black circles), compared with that of the corresponding Toeplitz matrix (red line), Eq. 30 for $\alpha = 1$ and $N = 200$.

corresponding to the smallest eigenvalue for $\beta = 0.2$, various values of α in the two regions ($\alpha_c(\beta = 0.2) \simeq 0.55$ in mean field approximation), and $N = 1000$. It can be observed that the slowest relaxation mode is confined to the left boundary, the more so the closer α to the dynamical transition, but no qualitative difference can be seen between region HD-II, where the rate depends on α , and HD-II', where the rate is independent of α .

The line $\alpha_c(\beta)$ separating the two regions (given, in the large N limit, by Eq. 30) is reported in Fig. 9 for $N = 800$ and compared with the pair and triplet approximations and exact and DWT results ($N = \infty$).

Dynamical transition in the pair and triplet approximations. The dynamical evolution equations characterizing the pair approximation, Eqs. 10–13, can be conveniently rewritten in matrix form by introducing the $(2N - 1)$ -component vector $x^t = (x_1^t, \dots, x_{2N-1}^t) = (\rho_1^t, J_1^t, \dots, \rho_{N-1}^t, J_{N-1}^t, \rho_N^t)$. Denoting by x_i the steady state value of x_i^t , and linearizing around x_i , we have

$$\dot{x}_i^t = - \sum_{j=1}^{2N-1} Q_{ij} (x_j^t - x_j), \quad i = 1, \dots, 2N - 1, \quad (31)$$

where Q is a pentadiagonal 2-Toeplitz [47] matrix whose eigenvalues have a positive real part. At odds with mean field, in this case we find that there are several pairs of complex conjugate eigenvalues. The smallest eigenvalue is real and is again the (slowest) relaxation rate λ or, equivalently, the inverse of the (longest) relaxation time of the dynamics. Unfortunately, we are not aware of any exact result for the spectrum of such a matrix. However we observe, on a purely numerical basis, that for $\alpha > \alpha_c(\beta)$ the ratio between the mean field rate and the pair one is nearly constant and very close to $\sqrt{2}$. In the case of the triplet approximation the matrix to consider is of course of order $4N - 5$ and the results are qualitatively similar.

In Fig. 8 we report the relaxation rate λ for $\beta = 0.2$ estimated by the pair and triplet approximation, together

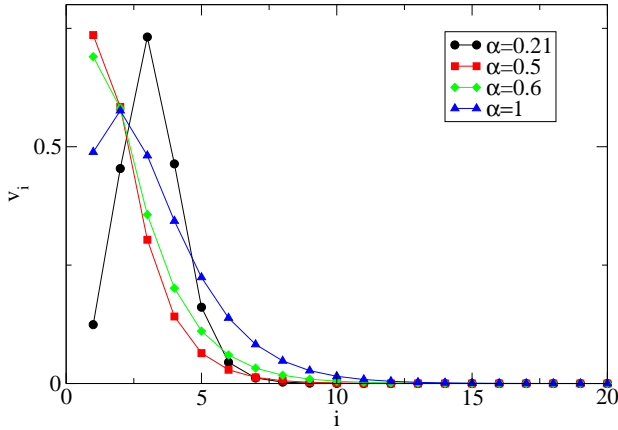


Fig. 7: Components v_i of the eigenvector corresponding to the smallest eigenvalue for $N = 1000$, $\beta = 0.2$ and $\alpha = 0.21$ (circles), 0.5 (squares), 0.6 (diamonds), 1 (triangles).

with the results from the mean field approximation, the DWT and the exact result. It can be observed that the pair and triplet approximations improve over the mean field one, considering both the rate value and the dynamical transition point $\alpha_c(\beta)$. The properties of the spectrum are similar to the mean field ones, that is for $\alpha > \alpha_c(\beta)$ the real parts of the eigenvalues form a “band” which tends to be continuous in a finite interval as N gets large, while for $\alpha \in (\beta, \alpha_c(\beta))$, the smallest eigenvalue detaches from the others and becomes α -dependent. Comparing with DWT results we see that mean field, pair and triplet overestimate the rate while DWT underestimates it (for $\alpha > 1/2$), and that even the triplet approximation does not reach the same accuracy as DWT. It is however interesting to note that the pair and triplet approximations provide a non-trivial (and improved with respect to mean-field) estimate of the dynamical transition point $\alpha_c(\beta)$, which in DWT is given by $1/2$, independent of β .

The dynamical transition line $\alpha_c(\beta)$ separating region HD-II from HD-II’ is reported in Fig. 9 and compared with mean-field, DWT and exact results.

Discussion. – We have shown how cluster approximations, based on suitable factorizations of the probability distribution at a given time, can be applied to the TASEP model with open boundaries. In particular we have considered the pair and triplet approximations (which have been previously applied to other models and called respectively (2,1) and (3,2) approximations in [4], and “triplet” and “quintuplet” approximations in [12]), and compared their results with mean-field, exact and DWT results.

We have observed that cluster approximations systematically give a quantitative improvement with respect to mean-field results, though retaining qualitative mean-field features. From a computational point of view, the resources needed for both mean-field and cluster approximations are negligible with respect to simulations.

We have focused in particular on the recently discovered

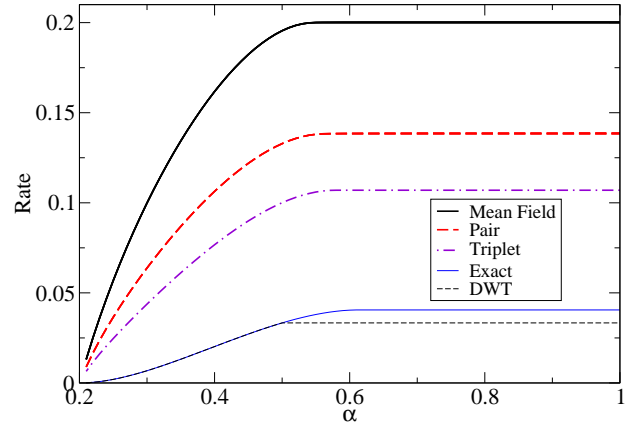


Fig. 8: Relaxation rate λ for $\beta = 0.2$ as a function of the injection rate α . From top to bottom: mean field (full line), pair approximation (dashed), triplet (dot-dashed), exact (thin full line) and DWT (thin dashed line) results. For the mean field, pair and triplet approximations, results for $N = 100, 200, 400, 800$ are reported, but the differences are smaller than the line thickness.

dynamical transition, which has been shown [43] to be particularly challenging for numerical simulations. Here even simple mean-field gives interesting results, in particular concerning the spectrum of the relaxation matrix. It is worth observing that our mean-field result for the dynamical transition is more accurate than the one given by the Burgers equation approach [43]. Pair and triplet approximations improve over mean-field and give a non-trivial estimate of the transition point $\alpha_c(\beta)$, which indeed depends on β , at odds with the DWT result.

The results we have obtained suggest that is worthwhile to apply these techniques to generalizations of the TASEP model for which exact results are limited or not available, like the Partially Asymmetric Simple Exclusion Process [34] or the TASEP with Langmuir kinetics [48, 49].

Author contribution statement. – The two authors contributed equally to the paper.

REFERENCES

- [1] VAN KAMPEN N., *Stochastic Processes in Physics and Chemistry* (Elsevier, Amsterdam) 2007
- [2] KAWASAKI K., *Phase Transitions and Critical Phenomena*, edited by C. DOMB and M. S. GREEN, Vol. 2 (Academic, London) 1972, p. 443
- [3] SCHADSCHNEIDER A., CHOWDHURY D. and NISHINARI K., *Stochastic Transport in Complex Systems* (Elsevier, Amsterdam) 2011
- [4] BEN-AVRAHAM D. and KÖHLER J., *Phys. Rev. A*, **45** (1992) 8358
- [5] SCHRECHENBERG M., SCHADSCHNEIDER A., NAGEL K. and ITO N., *Phys. Rev. E*, **51** (1995) 2939
- [6] BOCCARA N., *Modeling Complex Systems* (Springer, New York) 2004

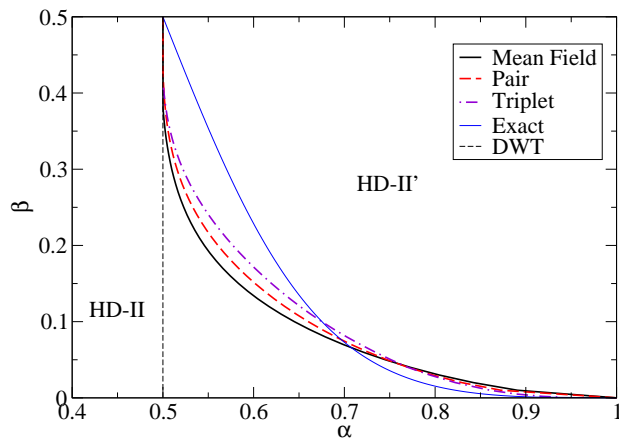


Fig. 9: The line $\alpha_c(\beta)$ separating region HD-II from HD-II'. Mean field ($N = 800$, full line), pair ($N = 800$, dashed), triplet ($N = 800$, dot-dashed), exact (thin full line) and DWT (thin dashed line) results.

- [7] GUTOWITZ H.A., VICTOR J.D. and KNIGHT B.W., *Physica D*, **28** (1987) 18
- [8] CRISANTI A., PALADIN G. and VULPIANI A., *Products of Random Matrices in Statistical Physics* (Springer, Berlin) 1983
- [9] GOUYET J.-F., PLAPP M., DIETERICH W. and MAASS P., *Adv. Phys.*, **52** (2003) 523
- [10] PETERMANN T. and DE LOS RIOS P., *J. Theor. Biol.*, **229** (2004) 1
- [11] PETERMANN T. and DE LOS RIOS P., *Phys. Rev. E*, **69** (2004) 066116
- [12] SCHWEITZER F. and BEHERA L., *Entropy*, **17** (2015) 7658
- [13] KIKUCHI R., *Phys. Rev.*, **124** (1961) 1682
- [14] KIKUCHI R., *Prog. Theor. Phys. Suppl.*, **35** (1966) 1
- [15] ISHII T., *Prog. Theor. Phys. Suppl.*, **115** (1994) 243
- [16] DUCASTELLE F., *Prog. Theor. Phys. Suppl.*, **115** (1994) 255
- [17] WADA K. and KABURAGI M., *Prog. Theor. Phys. Suppl.*, **115** (1994) 273
- [18] KIKUCHI R., *Phys. Rev.*, **81** (1951) 988
- [19] AN G., *J. Stat. Phys.*, **52** (1988) 727
- [20] PELIZZOLA A., *J. Phys. A: Math. Gen.*, **38** (2005) R309
- [21] ZAMPARO M. and PELIZZOLA A., *J. Stat. Mech.*, (2006) P12009
- [22] MÉZARD M. and MONTANARI A., *Information, Physics and Computation* (Oxford University Press) 2009
- [23] NERI I. and BOLLÉ D., *J. Stat. Mech.*, (2009) P08009
- [24] KANORIA Y. and MONTANARI A., *Ann. Appl. Prob.*, **21** (2011) 1694
- [25] AURELL E. and MAHMOUDI H., *J. Stat. Mech.*, (2011) P04014
- [26] AURELL E. and MAHMOUDI H., *Comm. Theor. Phys.*, **56** (2011) 157
- [27] AURELL E. and MAHMOUDI H., *Phys. Rev. E*, **85** (2012) 031119
- [28] LOKHOV A.Y., MÉZARD M. and ZDEBOROVÁ L., *Phys. Rev. E*, **91** (2015) 012811
- [29] DEL FERRARO G. and AURELL E., *Phys. Rev. E*, **92** (2015) 010102
- [30] SHRESTHA M., SCARPINO S.V. and MOORE C., *Phys. Rev. E*, **92** (2015) 022821
- [31] PELIZZOLA A., *Eur. Phys. J. B*, **86** (2013) 120
- [32] DOMINGUEZ E., DEL FERRARO G. and RICCI-TERSENGHI F., *J. Stat. Mech.*, (2017) P033303
- [33] PELIZZOLA A. and PRETTI M., *arXiv:1702.06822 [cond-mat.stat-mech]*, (2017)
- [34] CHOU T., MALLICK K. and ZIA R.K.P., *Rep. Prog. Phys.*, **74** (2011) 116601
- [35] MACDONALD C.T., GIBBS J.H. and PIPKIN A.C., *Biopolymers*, **6** (1968) 1
- [36] KRUG J., *Phys. Rev. Lett.*, **67** (1991) 1882
- [37] DERRIDA B., DOMANY E. and MUKAMEL D., *J. Stat. Phys.*, **69** (1992) 667
- [38] SCHÜTZ G. and DOMANY E., *J. Stat. Phys.*, **72** (1993) 277
- [39] DERRIDA B., EVANS M.R., HAKIM V. and PASQUIER V., *J. Phys. A: Math. Gen.*, **26** (1993) 1493
- [40] DERRIDA B., *Phys. Rep.*, **301** (1998) 65
- [41] DEGIER J. and ESSLER F.H.L., *Phys. Rev. Lett.*, **95** (2005) 240601
- [42] DEGIER J. and ESSLER F.H.L., *J. Phys. A: Math. Theor.*, **41** (2008) 485002
- [43] PROEME A., BLYTHE R.A. and EVANS M.R., *J. Phys. A: Math. Theor.*, **44** (2011) 035003
- [44] SMITH G.D., *Numerical Solution of Partial Differential Equations* (Clarendon Press, Oxford) 1978
- [45] DUDZIŃSKI M. and SCHÜTZ G.M., *J. Phys. A: Math. Gen.*, **33** (2000) 8351
- [46] NAGY Z., APPERT C. and SANTEN L., *J. Stat. Phys.*, **109** (2002) 623
- [47] GOVER M.J.C. and BARNETT S., *IMA J. Numer. Anal.*, **5** (1985) 101
- [48] PARMEGGIANI A., FRANOSCH T. and FREY E., *Phys. Rev. Lett.*, **90** (2003) 086601
- [49] PARMEGGIANI A., FRANOSCH T. and FREY E., *Phys. Rev. E*, **70** (2004) 046101